

Magnetoelastic effects in doped Fe₂PZ. Gercsi,¹ E. K. Delczeg-Czirjak,² L. Vitos,³ A. S. Wills,⁴ A. Daoud-Aladine,⁵ and K. G. Sandeman¹¹*Department of Physics, Blackett Laboratory, Imperial College London, London SW7 2AZ, United Kingdom*²*Division of Materials Theory, Department of Physics and Astronomy, Uppsala University, Box 516, SE 75120 Uppsala, Sweden*³*Applied Materials Physics, Department of Materials Science and Engineering, Royal Institute of Technology, SE-100 44 Stockholm, Sweden*⁴*Department of Chemistry, University College London, 20 Gordon Street, London WC1H 0AJ, United Kingdom*⁵*ISIS facility, Rutherford Appleton Laboratory, Chilton, Didcot, Oxfordshire, OX11 0QX, United Kingdom*

(Received 19 March 2013; revised manuscript received 26 June 2013; published 18 July 2013)

We use combined high resolution neutron diffraction (HRPD) with density functional theory (DFT) to investigate the exchange striction at the Curie temperature (T_C) of Fe₂P and to examine the effect of boron and carbon doping on the P site. We find a significant contraction of the basal plane on heating through T_C with a simultaneous increase of the c axis that results in a small overall volume change of $\sim 0.01\%$. At the magnetic transition the Fe_{*l*}-Fe_{*l*} distance drops significantly and becomes shorter than Fe_{*l*}-Fe_{*l+1*}. The shortest metal-metalloid (Fe_{*l*}-P_{*l*}) distance also decreases sharply. Our DFT model reveals the importance of the latter as this structural change causes a redistribution of the Fe_{*l*} moment along the c axis (Fe-P chain). We are able to understand the site preference of the dopants, the effect of which can be linked to the increased moment on the Fe_{*l*} site, brought about by strong magnetoelasticity and changes in the electronic band structure.

DOI: [10.1103/PhysRevB.88.024417](https://doi.org/10.1103/PhysRevB.88.024417)

PACS number(s): 75.30.Sg, 75.30.Kz, 75.80.+q, 75.30.Et

I. INTRODUCTION

Fe₂P-based magnetic alloys attract interest from many areas of physics, materials science, and geophysics research. They are found in meteorites and are considered as a candidate minor phase present in the Earth's core.^{1,2} An understanding of the mechanism of formation of these minerals can help to identify the histories of planetary bodies and the composition of the Earth's outer core. In LiFePO₄-based battery materials, a percolating nanonetwork of metal-rich phosphides including Fe₂P can significantly enhance electrical conductivity.³ Fe₂P-based alloys can furthermore be prepared as one-dimensional nanowires and nanocables.⁴ Of most relevance to this article, however, is the prospect of hexagonal Fe₂P-based alloys being used as room temperature magnetic refrigerants.

Fe₂P exhibits a first order magnetic transition from a ferromagnetic (FM) state to a paramagnetic one (PM) at 217 K accompanied by a significant change in the c/a ratio of the hexagonal structure. The paramagnetic susceptibility deviates from the Curie-Weiss law for temperatures well above T_C (up to 700 K).⁵ In nanocable form, the magnetic transition temperature is shifted 10–50 K higher compared to the parent composition because of strong strain and/or carbon doping.⁴ The increase in the T_C with only a small, partial replacement of phosphorus with other p -block elements (B, Si, or As) is remarkable. 10% replacement of P by B leads to $\sim 120\%$ change, while the same amount of Si and As substitution also results in a $\sim 70\%$ and $\sim 60\%$ increase (Fig. 1) respectively, with a simultaneous change in the nature of the transition from first order to second order.^{6–8} Such large changes in T_C are not restricted to doping by p -block elements. Partial replacement of Fe by Mn results in a significant increase of the saturation magnetization, while the first order nature of the metamagnetic transition is preserved up to and beyond room temperature and is tuned by magnetic field at a rate of ~ 3 KT⁻¹.^{9,10}

The metamagnetism of Fe₂P shares many features with the itinerant electron metamagnetism of La(Fe,Si)₁₃.¹¹ That material also has a PM to FM transition, the temperature

of which can be tuned from around 190 K to well above 300 K. The high magnetization state can be induced by a magnetic field above T_C , and the metamagnetic transition is tuned by field at a rate of around 4 KT⁻¹. As in Fe₂P the first or second order nature of its metamagnetism depends on the substituent (e.g., Co or Mn) or intercalating atom (e.g., H or C).^{12,13} Fe₂P-based and La(Fe,Si)₁₃-based alloys are two of the leading contenders for scale-up as magnetic refrigerants, due to their tunable metamagnetism, their large room temperature magnetocaloric effect (MCE), and the fact that they are mostly composed of abundantly available 3d and p -block elements.¹⁴

There has been a recent growth in theoretical investigations of the origin and tunability of metamagnetism in Fe₂P and of the appearance of a body centered orthorhombic structure in substituted alloys. This is partly motivated by the sensitivity to doping of the T_C and any associated thermomagnetic hysteresis, and given added impetus more recently by the investigation of the MCE of industrially-scaled quantities of material where good compositional tolerance is required. A Landau-Ginzburg free energy analysis based on fixed-spin-moment calculations that took into account the effect of spin fluctuations revealed the metamagnetic nature of the Fe-atoms at a particular crystallographic ($3f$) site in the parent alloy as well as in the doped counterparts.^{15,16} Using linear muffin tin orbitals in the atomic sphere approximation, Severin *et al.*¹⁷ found that the magnetic moments in the inter-related hexagonal and orthorhombic structures are very similar and scale with the nearest-neighbor Fe-P distances. We recently found that the phonon vibrational free energy stabilizes the hexagonal phase, whereas the electronic and magnetic entropies favor a low symmetry orthorhombic structure in Si-substituted Fe₂P_{1-x}Si_x alloys.¹⁸ An analysis of the exchange constants in the hexagonal structure of B-, Si-, and As-doped Fe₂P helps to explain trends in Curie temperature. A principal interlayer Fe-Fe interaction was identified as controlling the strength of ferromagnetism.¹⁹ Recently, Liu *et al.* also linked the metamagnetic transition of the Fe moment at the 3f site to

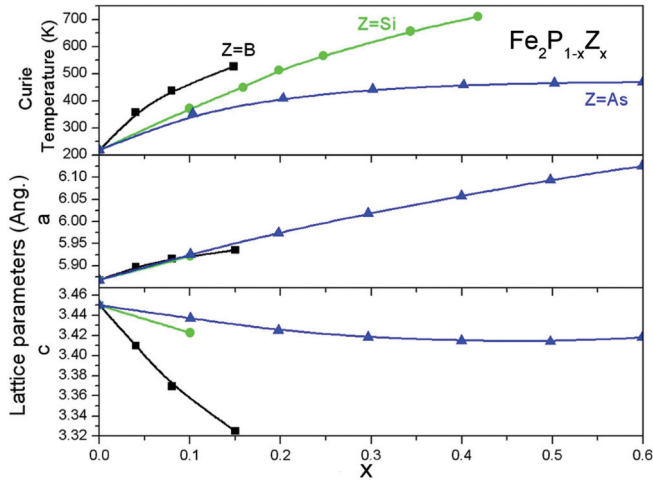


FIG. 1. (Color online) The effect of boron, silicon and arsenic doping in $\text{Fe}_2\text{P}_{1-x}\text{Z}_x$ on the magnetic ordering temperature T_C (top) and the room temperature lattice parameters (bottom).⁶⁻⁸

the critical Fe-Fe distances using exchange coupling analysis based on DFT.²⁰

In the present paper we employ a joint experimental-theoretical approach that we have used elsewhere to uncover the microscopic mechanism of metamagnetism in Mn-based antiferromagnets. By using DFT in combination with structural information from HRPD²¹ we have previously mapped the magnetic phase diagram of Mn-based metallic orthorhombic compounds in the $Pnma$ space group as a function of Mn-Mn distance²² and have predicted new antiferromagnetic metamagnets.^{23,24} HRPD indicated the most relevant changes in the interatomic distances which was then mimicked by *ab initio* simulations to compare the total energies of the competing magnetic states. Taking a similar approach here, we first analyze and compare the peculiar magnetoelastic coupling of the metamagnetic transition in Fe_2P , in boron-doped $\text{Fe}_2(\text{P,B})$ and in carbon-doped $\text{Fe}_2(\text{P,C})$ using HRPD. In the second part of the paper, we use a simple DFT model to further interpret the large interatomic changes at the magnetic transition. Our aim is to provide clues as to how to control and optimize the structure-magnetism relationship in this highly tunable materials class.

II. PREVIOUS EXPERIMENTAL FINDINGS

Fe_2P is the prototype structure of the hexagonal space group 189 ($P\bar{6}2m$) with nine atoms in the unit cell. The six Fe atoms occupy two nonequivalent threefold symmetry sites (3f and 3g), while the phosphorus atoms sit on a singlefold (1b) and on a twofold position (2c) in the crystal lattice. Here we adopt the following established notation: Fe_I for the 3f ($x_I, 0, 0$) positions, Fe_{II} for the 3g ($x_{II}, 0, 1/2$) positions, and P_I and P_{II} for the 2c ($1/3, 2/3, 0$) and 1b ($0, 0, 1/2$) positions of the P atoms, respectively. The hexagonal cell is composed of triangles in the ab plane as shown in Fig. 2. The iron atoms that alternate along the c axis are surrounded either by four P atoms with tetrahedral symmetry (Fe_I) or by five P atoms forming a pyramid (Fe_{II}). It was reported previously²⁵ that the c -axis lattice parameter increases with temperature

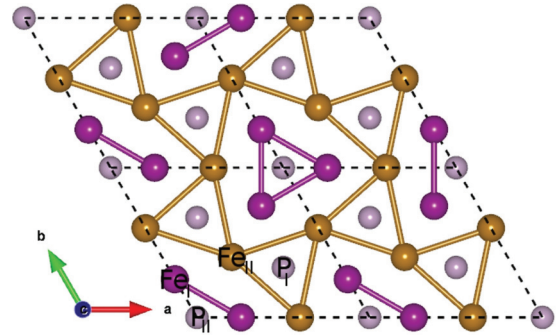


FIG. 2. (Color online) Atomic arrangement of the Fe_2P in the basal plane. Fe atoms occupy two nonequivalent threefold symmetry sites, 3f (Fe_I) and 3g (Fe_{II}), and the phosphorus atoms sit on a singlefold 1b (P_I) and twofold position, 2c (P_{II}) in the hexagonal crystal lattice. Fe_I ($x_I, 0, 0$) atoms share the same plane with P_I ($1/3, 2/3, 0$) and Fe_{II} atoms ($x_{II}, 0, 1/2$) with P_{II} ($0, 0, 1/2$), respectively.

while the a and b axes (basal plane) exhibit negative thermal expansion. The same authors used a strain gauge dilatometer to measure the linear thermal expansion ($\Delta l/l$) of a single crystal of Fe_2P upon cooling through the first order type magnetic transition and found a sharp increase of $\frac{\Delta a}{a} = 0.74 \times 10^{-3}$ with the simultaneous decrease of the c axis: ($\frac{\Delta c}{c} = -0.84 \times 10^{-3}$).

The coupling between the structure and magnetism is further manifested by the effect of doping shown in Fig. 1. A significant increase in Curie temperature upon partial replacement of the P atoms by other p -block elements such as B, Si, and As has been observed.⁶⁻⁸ Catalano *et al.*⁶ investigated the effect of isovalent substitution of As for P on the crystalline lattice and on magnetic properties. The authors found that the larger atomic radius As can be continuously accommodated into the hexagonal lattice between $0 \leq x \leq 0.65$ in $\text{Fe}_2\text{P}_{1-x}\text{As}_x$ with a strong site preference for the P_I (2c) position. The monotonic increase of the lattice volume with As addition is a compromise of a moderate increase of a axis and a simultaneous contraction of the lattice along the c direction. The same tendency was observed by the substitution of larger atomic radius, nonisovalent Si for P by Jernberg *et al.*⁸ Interestingly, Si atoms were also found to show some site preference for the P_I position with opposing trends in the a and c lattice parameters and a significant increase in the magnetic ordering temperature. Silicon addition above $x \leq 0.1$ results in a change from the hexagonal lattice structure into one with a body-centered orthorhombic, $Imm2$ (44) symmetry.

Finally, the partial replacement of P by the substantially smaller atomic radius boron results in a remarkable increase of the T_C . The solid solubility of the B atoms in $\text{Fe}_2\text{P}_{1-x}\text{B}_x$ is, however, limited to $x \approx 0.15$ due to the formation of other Fe_5PB_2 , Fe_3B , and Fe_2B refractory borides at higher B concentrations. Chandra *et al.* established by means of Mössbauer spectroscopy that the small boron atoms, unlike the larger elements (As and Si), occupy the P_{II} (1b) singlefold position in the hexagonal lattice.⁷ Another consequence of the chemical pressure on the hexagonal lattice caused by boron addition as compared to the parent alloy or to the Si/As-doped compositions is decreased lattice volume. Despite such differences, the monotonic increase of the a and decrease

of the c lattice parameters of the unit cell is strikingly similar to the effect of larger p -element dopants (Fig. 1). An additional consequence of boron doping is that the first-order PM-FM transition of undoped Fe₂P becomes second order.

III. METHODS

A. Experimental methods

The samples used in this study were prepared from ultrahigh purity elements. The powders were mixed to weight ratios to according to nominal compositions of Fe₂P and Fe₂P_{0.96}Z_{0.04}, (Z = B or C) and then thoroughly ground together in an agate mortar under protective atmosphere. The initial powders were then pressed into pellets and sealed into quartz ampoules under protective argon atmosphere for solid state reaction. The initial annealing temperature was raised slowly (0.5 K min⁻¹) up to 673 K, where each sample was kept for four hours for an initial reaction. There was a subsequent heating step (at 1 K min⁻¹) up to 1273 K where the temperature was held for a further four hours. An additional heat treatment at 973 K for four hours was applied before the sample was oven-cooled to room temperature. X-ray diffractometry was used to evaluate the structural properties of the prepared samples. Single phase hexagonal compositions were found in all specimens by this method. Neutron diffraction was carried out at the time-of-flight high resolution powder diffractometer at ISIS, UK. This instrument has a resolution of $\frac{\Delta d}{d}$ of 10⁻⁴ and was used at temperatures between 4.2 and 550 K. Neutron diffraction found some traces of unreacted carbon in Fe₂P_{0.96}C_{0.04} which we here refer to as a nominal composition since the actual carbon concentration of the main phase will be somewhat smaller. Magnetic properties were measured between 10 and 400 K in a Quantum Design Physical Properties Measurement System.

B. Computational model

The electronic structure calculations were performed using the Vienna *ab initio* simulation package (VASP) code, based on DFT within projector augmented wave method²⁶ with Perdew-Burke-Ernzerhof parametrization.²⁷ Site-based magnetic moments were calculated using the Vosko-Wilk-Nusair interpolation²⁸ within the general gradient approximation for the exchange-correlation potential. A k -point grid of 11 × 11 × 13 was used to discretize the first Brillouin zone and the energy convergence criterion was set 10⁻⁷ eV during the energy minimization process. The density of states (DOS) plots presented in this work were calculated on a dense (19 × 19 × 21) k grid for high accuracy. The spin-orbit interaction was turned off during the calculations and only collinear FM and nonmagnetic (NM) configurations were considered.

The minimal, nine-atom basis cell (six Fe atoms and three P atoms) was used to evaluate the total energies and magnetic properties of the alloys. Using this simple model, the effect of doping was simulated by the replacement of a single phosphorous atom by another p -block element (Z) that represents an $x = 1/3$ compositional change in the Fe₂P_{1-x}Z_x formula. Although this approach is undoubtedly oversimplified in respect of exact compositions provided in the experimental section, we believe it is still a suitable model to

capture the relevant changes in the electronic structure caused by the dopant elements. In order to be consistent with the experimental results, we only considered changes along the a and c axis by the individual expansion and compression of the a - and c -lattice parameters, without allowing any relaxation of the strained structure. In practice, we varied the lattice parameters using a step size of $\pm 0.5\%$, calculating the self-consistent electronic structures at each step.

IV. RESULTS

A. Magnetometry

The samples were first cooled to 10 K, where magnetization curves were collected at fields up to 5 T, after which thermomagnetic curves were collected on heating to 400 K in an applied field of 0.01 T. The results are plotted in Fig. 3. The parent alloy shows a sharp, first order transition at $T \approx 215$ K in accordance with values reported previously. The strong effect of doping on the magnetic order temperature is apparent. As expected, the partial replacement of P by the much smaller atomic radius B significantly increases T_C . In this study, we also partially replaced P by C atoms for the first time. The empirical atomic radius of carbon is much smaller (70 pm) than that of the phosphorus (100 pm) and boron (85 pm) elements. On the other hand, in terms of valence electrons the sequence B(p^1) < C(p^2) < P(p^3) stands. In practice, carbon doping shows a very similar effect to that of the other p -block substituents as it also clearly increases the magnetic order temperature. Furthermore, the Curie transition is heavily broadened by doping as demonstrated by the smearing out of the temperature derivative of the magnetization ($\frac{\partial M}{\partial H}$) (Fig. 3). Finally, the saturation magnetization (M_S) increases slightly with doping; $M_S = 112, 113,$ and 116 Am²/kg was obtained for Fe₂P, Fe₂P_{0.96}C_{0.04}, and Fe₂P_{0.96}B_{0.04}, respectively, at 10 K in 9 T applied magnetic field. This slight increase of M_S is in line with the expectations from DFT calculations (see

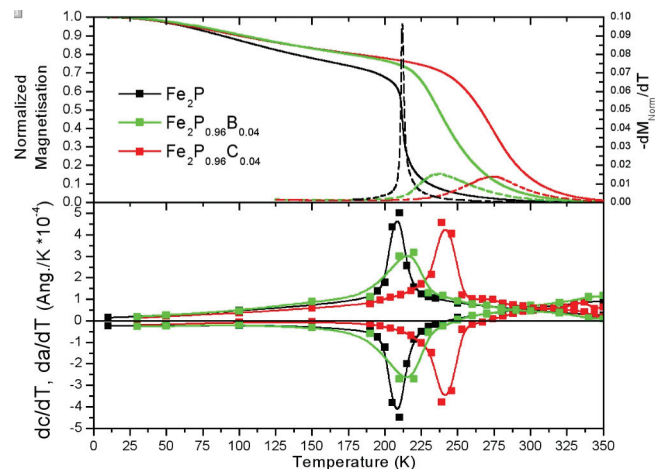


FIG. 3. (Color online) Thermomagnetic curves of the parent Fe₂P alloy with the C and B doped counterparts (top, left axis) in the field of $\mu_0 M = 0.01$ T. Derivatives ($\frac{dM}{dH}$) are linked to the right axis (top). Bottom figure shows the change of the lattice parameters (a, c) for comparison, obtained using HRPD.

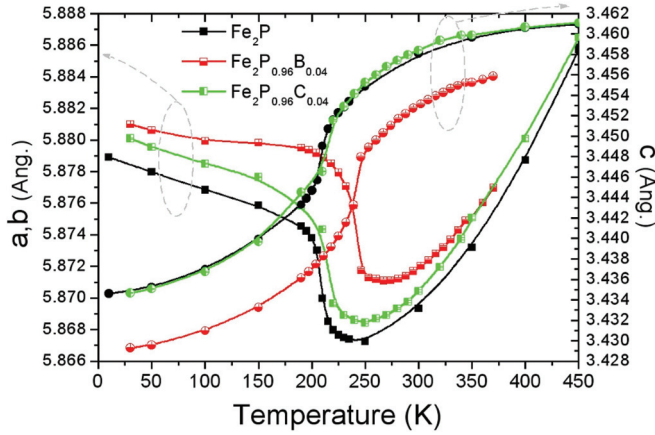


FIG. 4. (Color online) Temperature evolution of the lattice parameters of the parent Fe_2P compound together with that of the C- and B-doped samples. The strong magnetoelastic response is especially apparent around the magnetic ordering temperature (~ 215 K).

Sec. V B). However, the samples were not fully saturated due to the large magnetocrystalline anisotropy.⁵

B. High resolution neutron diffraction

Figure 4 shows the anisotropic lattice expansion of the a and c axes of Fe_2P and the doped compounds. In the magnetically ordered state ($T \lesssim 200$ K) the basal plane exhibits negative lattice expansion with increasing temperature. When the temperature reaches T_C , a sharp contraction of the lattice in the ab plane is observed. The a -lattice expansion only looks Debye-like at higher temperatures ($T \gtrsim 240$ K) in the paramagnetic phase. On the other hand, the thermal expansion of the c axis is found to be positive over the entire investigated temperature range. The magnetic ordering temperature is also strongly reflected in the lattice response along c . The consequence of these counteracting lattice parameter changes over the magnetic transition is a volume change at T_C which is as small as 0.01%.

The effect of doping on the lattice parameters is clear; the basal plane of the hexagonal lattice expands while the c axis shows contraction. At first glance, the anomalous thermal lattice expansion resembles that of the parent alloy. However, temperature derivatives of these quantities ($\partial a/\partial T$, $\partial c/\partial T$) reveal characteristic differences between the parent and doped alloys, shown in Fig. 3. The sharpness of the derivatives demonstrates the first order nature of the magnetoelastic transition of stoichiometric Fe_2P . Although $\partial a/\partial T$ and $\partial c/\partial T$ are of opposite sign, they both have sharp peaks at temperature $T_p = 209$ K. Both B and C doping cause a shift of T_p to higher temperatures with broader $\partial a/\partial T$ and $\partial c/\partial T$. These effects on the lattice properties correspond very well to the observed changes in the magnetic properties. The temperature derivative of the magnetization in Fig. 3 (top), reveals similar broadening of the ferromagnetic transition with B or C doping.

HRPD is capable of tracking the change in the interatomic distances, thus providing information about the magnetoelastic coupling in these materials. The evolution of the lattice parameters through the magnetoelastic transition is already a clear indication of the significant changes of the atomic distances. Both the 3f and 3g positions of the iron atoms

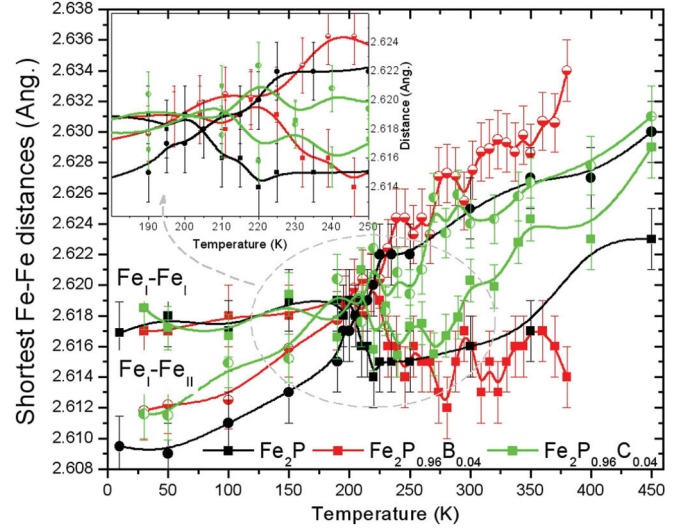


FIG. 5. (Color online) The shortest $\text{Fe}_I\text{-}2\text{Fe}_I$ and $\text{Fe}_I\text{-}2\text{Fe}_{II}$ distances as a function of temperature for all investigated samples. Inset depicts the temperature region of the crossover.

are low symmetry positions described by the positional parameters x_I and x_{II} , respectively. Iron atoms on the 3f site (Fe_I) are connected to two other iron atoms of the same type, denoted as $\text{Fe}_I\text{-}2\text{Fe}_I$. There are also two distinctive $\text{Fe}_I\text{-}2\text{Fe}_{II}$ and $\text{Fe}_I\text{-}4\text{Fe}_{II}$ connections to iron atoms located at the 3g site (Fe_{II}). Finally, there exists a relatively close $\text{Fe}_{II}\text{-}4\text{Fe}_{II}$ distance above 3 Å. In Fig. 5, we only plot the two shortest distances, $\text{Fe}_I\text{-}2\text{Fe}_I$ and $\text{Fe}_I\text{-}2\text{Fe}_{II}$, as a function of temperature, evaluated from Rietveld refinements of the HRPD data. In all of the investigated samples, the $\text{Fe}_I\text{-}2\text{Fe}_{II}$ distance is the shortest Fe-Fe separation at low temperatures (< 200 K). The latter increases with temperature, eventually becoming larger than the $\text{Fe}_I\text{-}2\text{Fe}_I$ distance, which is strongly reduced in the vicinity of the magnetic transition temperature. The point in temperature above which $\text{Fe}_I\text{-}2\text{Fe}_I$ is the shortest Fe-Fe distance is between 190 and 220 K for all samples.

In addition we can distinguish two groups of metal-metalloid distances: $\text{Fe}_I\text{-}(\text{P}_I, \text{P}_{II})$ and $\text{Fe}_{II}\text{-}(\text{P}_I, \text{P}_{II})$. The shortest one is $\text{Fe}_I\text{-}2\text{P}_I$, followed by $\text{Fe}_I\text{-}2\text{P}_{II}$, $\text{Fe}_{II}\text{-}\text{P}_{II}$, and $\text{Fe}_{II}\text{-}4\text{P}_I$. Figure 6 contains the two shortest distances only. The separation of $\text{Fe}_{II}\text{-}\text{P}_{II}$ and $\text{Fe}_{II}\text{-}4\text{P}_I$ atoms is in the range of ~ 2.37 Å and ~ 2.49 Å, respectively. It is worth noting that both $\text{Fe}_I\text{-}2\text{P}_I$ and $\text{Fe}_{II}\text{-}\text{P}_{II}$ (not shown) only have components within the ab plane which explains the resemblance of their temperature evolution to that of the a lattice parameter in Fig. 4: The shortest $\text{Fe}_I\text{-}2\text{P}_I$ distance decreases sharply on heating through the magnetic transition in the parent alloy as well as in the doped compounds. Its significance will be discussed in the context of our theoretical results in the next section. The larger a lattice parameter in the doped compounds means that the Fe-P distance is largest in those samples.

V. THEORETICAL RESULTS

A. Stoichiometric Fe_2P

We now use a zero temperature theoretical model to explore the effect of changing the lattice structure on the magnetization

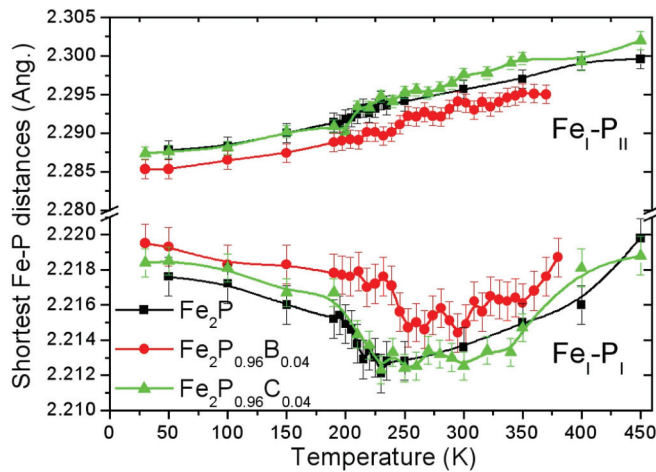


FIG. 6. (Color online) The shortest metal-metalloid distances, Fe_I-2P_I and Fe_I-2P_{II} , as a function of temperature in Fe_2P together with the doped counterparts. Both distances relate to the metamagnetic 3f (Fe_I) site.

of Fe_2P in this subsection and of the doped compounds in the following section. Our aim is to establish the most significant contributions to the magnetoelastic coupling in this material family. The calculated variation of total magnetization in the FM state with lattice parameters is plotted in Fig. 7. A small change in the lattice can have a very strong effect on the magnetic properties. The lattice expansion within the basal plane causes the total magnetic moment/formula unit to increase abruptly from $\sim 1.3 \mu_B$ to $3.1 \mu_B$ around a critical value of $a \approx 5.7 \text{ \AA}$, and stays practically constant above it. The magnetization varies very little with c , reflecting the greater importance of the atomic distances within the basal plane, where the atoms are packed more densely. The calculations reveal the unusual duality of the magnetic structure of Fe_2P in which there is a large magnetic moment of $M(Fe_{II}) = 2.16 \mu_B$ on the 3g site together that coexists with a significantly smaller, $M(Fe_I) = 0.85 \mu_B$, moment on the 3f crystallographic site. These findings are in full agreement with previous studies (see

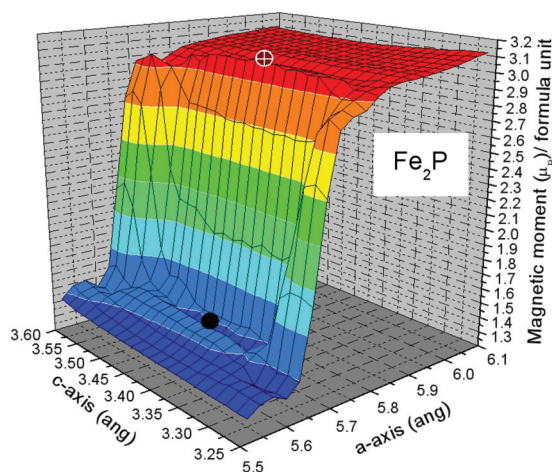


FIG. 7. (Color online) Total magnetic moment/formula unit as a function of lattice parameter of Fe_2P . The magnetic moment is strongly linked to the change in a -lattice parameter. The red and black dots indicate the high and low magnetization states (see text).

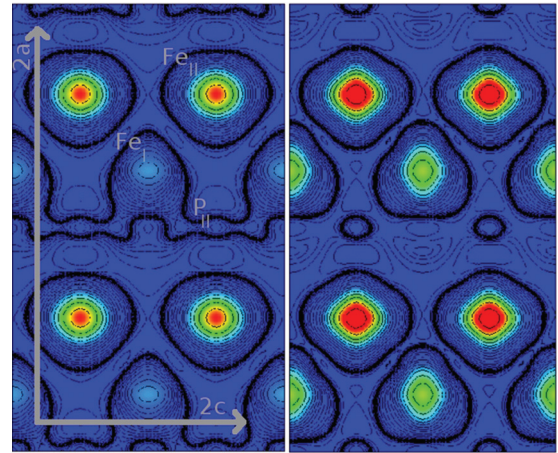


FIG. 8. (Color online) A comparison of the spin density of the low magnetization state (left) and high magnetization state (right) and of Fe_2P . The large magnetic moment around the Fe_{II} site is only decreased in amplitude above the transition, when strong delocalization of the Fe_I magnetization occurs simultaneously.

Sec. II). Figure 8 compares the differences in spin densities of the high and low magnetic configurations (as indicated by the red and black dots in Fig. 7). As a consequence of the lattice symmetry, the shortest metal-metalloid distance, Fe_I-P_{II} , as well as the shortest metal-metal separation, Fe_I-Fe_{II} , have projections along both the a and c axes, and so this is the most suitable cross section for our analysis. If we consider solely the effect of the structural changes that we know to occur at the Curie transition (Fig. 5), we find that there is a redistribution of magnetization of the Fe_I site. The large and localized magnetic moment on the Fe_{II} site is decreased in amplitude to $\sim 1.3 \mu_B$ above the transition and strong delocalization of the Fe_I magnetization occurs simultaneously. Electrons from the Fe_I site that have a magnetic contribution are redistributed along the c axis in directions that link the Fe_I and P_{II} sites.

In Fig. 9, we compare the total electronic density of states of the high and low magnetization states, at (a, c) values indicated by the red and black dots in Fig. 7. The high magnetization state has a high and sharp DOS at E_F with $\sim 80\%$ spin polarization, dominated by minority (down) spins (Fig. 9, red line). When the lattice is compressed within the basal plane, the magnetization is significantly weakened, as shown in Fig. 7. The filled bands at low energy contain the phosphorus $3s$ states (not shown). The conduction band is formed by the $3d$ states of Fe and the $3p$ states of P as is typical of strong $p-d$ hybridization. The hybridized states are also present near the Fermi level, influencing the exchange splitting of the $3d$ states of Fe. The effect of the smaller a -lattice parameter (in the low magnetization state) is to reduce the exchange splitting considerably. The high peaks in the majority (up spin) DOS located around -0.5 eV are shifted to -0.2 eV . In the minority DOS, the opposite trend is observed as the triple peak feature between 0 and 0.25 eV is lowered to around -0.25 eV .

We can ascribe three competing effects to the magnetoelastic transition. From our experiment, with increasing temperature the separation between Fe_I and Fe_{II} atoms increasing monotonically was observed (see Fig. 5). Our previous exchange coupling analysis¹⁹ found that the largest

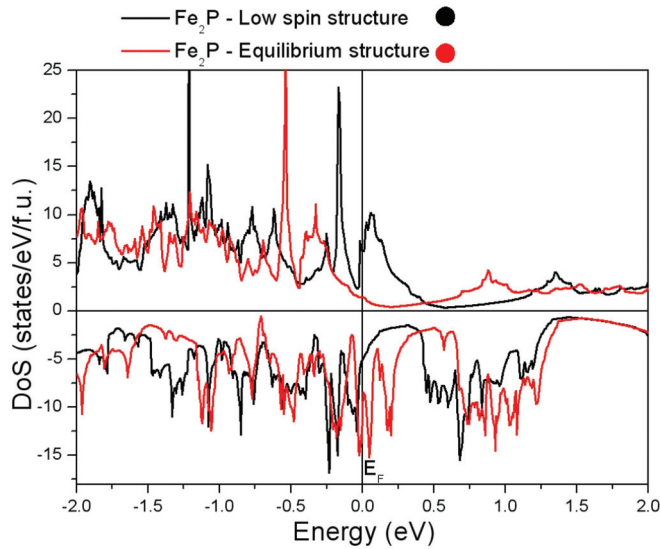


FIG. 9. (Color online) Comparison of the density of states of a high magnetization state (red) and a low magnetization state (black) in Fe_2P .

contribution to the decrease in the c/a ratio is the weakened magnetic interaction between the Fe atoms on 3f and 3g sites. Secondly, at the magnetic transition the $\text{Fe}_I\text{-Fe}_I$ distance is also altered and it becomes comparable to $\text{Fe}_I\text{-Fe}_{II}$ but the exchange constant between $\text{Fe}_I\text{-Fe}_I$ atoms is only the fraction of the $\text{Fe}_I\text{-Fe}_{II}$ exchange, and has a less pronounced dependence on distance. Thirdly, the shortest $\text{Fe}_I\text{-P}_I$ distance, located in the ab plane also decreases around the transition temperature. This results in a significantly stronger hybridization that can explain the decrease in magnetization and alternation of these bonds, and hence trigger a lattice distortion in the first place. A similar scenario was also drawn from the comparison of the total electronic charge density in the FM and PM states of Mn and Si doped Fe_2P -type alloy by Dung *et al.*⁹ In the following section, we compare the effect of doping on the structure and magnetic properties obtained by means of DFT using structural data from neutron diffraction.

B. The effect of doping

There exist two crystallographic sites where the metalloid elements can be incorporated into the lattice, albeit with strong site preference as described in Sec. II. Experimentally, elements with an atomic radius smaller than P were found to show a preference in the singlefold position (1b), whilst larger elements tend to occupy the twofold symmetry site (2c) in the hexagonal lattice. In order to establish the site preference from DFT calculations, we compare the difference in total energy for the different elemental substitution. First of all, the calculated total energies of the FM solutions [at any (a, c) lattice parameter value] were always found to be energetically more stable than that of the NM configurations by 1.5–3 eV/f.u., yielding a strong tendency toward the formation of magnetic order in all the investigated alloys. The site preference of the dopants can be established by calculating the difference in total energy (dE) between the singlefold and twofold site position occupancies using the equilibrium lattice

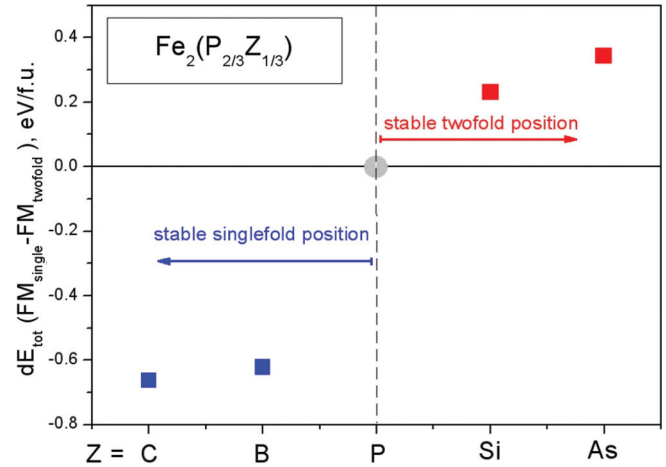


FIG. 10. (Color online) Site preference of the p -block dopants as established from DFT. Negative total energy differences represent preference for the singlefold position. Positive total energy differences suggest tendency for twofold site occupancy.

of the FM state. The calculations find a clear trend with the size of the substituents: The energy difference is negative for elements that are smaller than P (left hand side of Fig. 10), reflecting the preference for singlefold occupation. On the other hand, a substituent with larger atomic radii (Si and As) prefers to occupy the twofold position of the hexagonal lattice.

This theoretically established site occupation of the dopant elements is in line with the experimental findings (see Sec. II), suggesting the dominance of size effects. Therefore, we hereafter focus our magnetoelastic investigations on the effect of singlefold site occupation by the small C and B elements and the twofold site occupation of the large Si and As elements.

The effect of doping on the lattice parameters is shown in Fig. 11. The NM calculations (black line) show an increasing trend in both the a and c parameters of the hexagonal structure

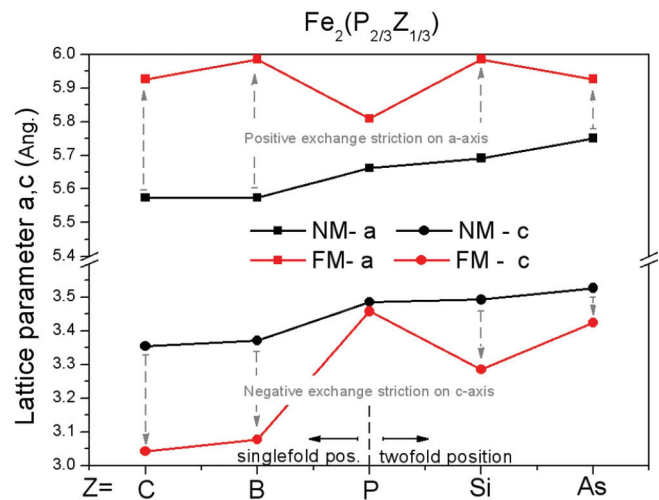


FIG. 11. (Color online) Equilibrium lattice parameters for NM and FM states as a result of DFT calculations as a function of dopants in $\text{Fe}_2\text{P}_{2/3}\text{Z}_{1/3}$, where $Z = \text{C, B, Si, or As}$, respectively.

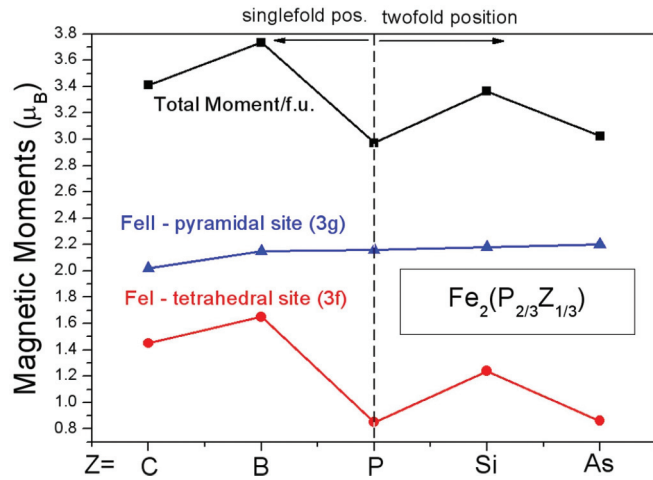


FIG. 12. (Color online) Total and site-projected magnetic moments in Fe₂P_{2/3}Z_{1/3}, for Z = C, B, Si, and As, respectively.

with the inclusion of larger atomic radius, anionic *p*-block elements. This behavior is easily anticipated in terms of chemical pressure as the lattice is expected to adapt according to the size of dopant. Examining Fig. 11, the steepest change in the lattice is seen with the partial replacement of P by B atoms, due to the largest difference in atom size between these elements. However, in the presence of FM interactions, any monotonic relation of lattice parameter to the atomic radius of the dopant is broken. The parent alloy has significantly smaller *a* and larger *c* parameters in the FM ground state than the doped compounds. The onset of ferromagnetism increases the separation of atoms within the basal plane (positive exchange striction) while their separation along the *c* axis is reduced (negative exchange striction), regardless of the size or valence state of the dopant as compared to the parent composition (Fe₂P). The overall volume change caused by the ferromagnetic exchange is positive, dominated by the larger *a* parameter [$V_{hex} = a^2c \sin(2\pi/3)$]. Based on these calculations, one would expect the lattice to expand along the *a* axis with a simultaneous contraction of the *c* axis in the vicinity of the magnetic ordering temperature. Indeed, experimental (HRPD) measurements clearly reveal this sharp positive exchange striction in the basal plane and the shrinkage of the *c* axis upon cooling the sample through the Curie temperature (see Fig. 4).

The significant coupling of the lattice to the magnetization also becomes apparent from the analysis of the total and site-projected magnetic moments as plotted in Fig. 12. The magnetic moment of Fe_{II} atoms show very little variation with doping and stays at around 2.2 μ_B. Although the larger *p*-block dopants increase the separation of the Fe_{II}-Fe_{II} atoms, this distance is typically above 3 Å, and so doping only slightly alters the exchange-split states. In strong contrast, the site-resolved magnetization of the 3f site is found to be much more sensitive to the valence electron number of the anionic elements. Examining Fig. 12 there is a strong relation between added valence electron number and magnetization with Z = B (−2e[−]), C (−1e[−]), P(−), Si (−2e[−]), or As(−). This feature can be explained in terms of charge transfer from Fe_I to the anionic Z element in order to fill the electronegative

p shell of the latter. The charge transfer is distance dependent and is strongly suppressed by the strong *p-d* interaction at smaller Fe_I-Z separations, while lattice expansion suppresses *p-d* hybridization and increases the degree of localization and ionic bonding in the system. With doping, the short Fe_I-Z distances are strongly influenced, altering the balance between magnetic moment formation (Fig. 8) and bond formation. The larger magnetic moments on the Fe_I atoms that result from doping account for the expansion of the basal plane as indicated by the comparison of Figs. 11 and 7.

VI. SUMMARY AND CONCLUSION

We have used high resolution neutron diffraction as well as density functional theory to investigate the effect of *p*-block element doping on the magnetoelastic properties of Fe₂P. HRPD has revealed that the strong coupling between the magnetism and the lattice is manifested by the contraction of the basal plane and by a significant increase of the *c* axis on heating through the magnetic transition, resulting in a small overall volume change of the lattice (>0.01%). A simultaneous change in both the metal-metal and metal-metalloid distances is observed.

DFT calculations reveal that the magnetic properties are strongly dependent on expansion in the basal (*ab*) plane, while they are almost invariant with regard to variation of the *c* parameter. The strong dependence of magnetic moments on the 3f site is related to the *a* lattice parameter that lies in the proximity of a critical value where change from low to high magnetization can occur. The closest metal-metal and metal-metalloid distances—the latter also linked to the metamagnetic 3f site—are strongly altered by both the *d-d* and *p-d* hybridization energies at the transition. As a result, the redistribution (delocalization) of the magnetization from the 3f site along the Fe_I-P_{II} chains in the *c*-axis direction occurs as shown in Fig. 8, implying its strong influence on bonding (also suggested by Dung *et al.*¹⁰) Our current analysis finds the survival of the magnetic moment on the 3g site above the magnetic transition. This is in line with our previous exchange interaction analysis¹⁹ which revealed anisotropic coupling, with strongly ferromagnetic Fe_{II}-Fe_{II} interactions accounting for the short range magnetic correlations and the observed divergence of Curie-Weiss law.^{5,10}

Our theoretical investigations on the effect of doping show that elements with an atomic radius smaller than phosphorus (e.g., C or B) occupy singlefold (1b) sites while larger elements such as Si or As prefer to occupy the twofold symmetry site (2c) in the hexagonal lattice. The moment on the 3g site is not influenced by the dopant and takes a high value (~2.2μ_B). By contrast, the iron atoms on the metamagnetic site develop smaller magnetic moments, the magnitude of which varies in direct relation to the valence electron number of the doping element. As a result, the conditions for the metamagnetic transition of the 3f site are locally modified by doping, resulting in a smearing of the transition as observed experimentally. Indeed, the increased exchange splitting on Fe_I results in increased exchange coupling parameters, significantly increasing the Curie temperature.¹⁹

Our DFT analysis finds that the magnetization is highly sensitive to the change in lattice dimensions, therefore both compositional inhomogeneities and internal strains as set by the preparation conditions can significantly alter the observed magnetic properties of the material.²⁹ For applications (such as magnetic refrigeration), where the transition temperature needs to be set by the material to a high accuracy, elements such as Si and As are favorable but process control will be crucial. Finally, as the remarkable change in magnetic ordering of these alloys is linked to the lattice parameters within the basal plane, uniaxial thin films on flexible substrates could be exploited to electrically manipulate the magnetic properties of this material system.

ACKNOWLEDGMENTS

We thank L. Szunyogh for useful discussions and D. Boldrin for help with sample preparation. We also thank K.S. Knight for providing us with the ¹¹B isotope used for this study. Financial support is acknowledged from The Royal Society (KGS) and EPSRC grant EP/G060940/1 (KGS and ZG). The research leading to these results has received funding from the European Community's 7th Framework Programme under Grant agreement 310748 "DRREAM". Figures 2 and 8 were prepared using VESTA open-source software.³⁰ Computing resources provided by Darwin HPC and Camgrid facilities at The University of Cambridge and the HPC Service at Imperial College London are gratefully acknowledged.

-
- ¹P. Dera, B. Lavina, L. A. Borkowski, V. B. Prakapenka, S. R. Sutton, M. L. Rivers, R. T. Downs, N. Z. Boctor, and C. T. Prewitt, *Geophys. Res. Lett.* **35**, L10301 (2008).
- ²H. P. Scott, B. Kiefer, C. D. Martin, N. Boateng, M. R. Frank, and Y. Meng, *High Press. Res.* **28**, 375 (2008).
- ³P. S. Herle, B. Ellis, N. Coombs, and L. F. Nazar, *Nat. Mater.* **3**, 147 (2004).
- ⁴J. Wang, Q. Yang, J. Zhou, K. Sun, Z. Zhang, X. Feng, and T. Li, *Nano Research* **3**, 211 (2010).
- ⁵H. Fujii, T. Hōkabe, T. Kamigaichi, and T. Okamoto, *J. Phys. Soc. Jpn.* **43**, 41 (1977).
- ⁶A. Catalano, R. J. Arnott, and A. Wold, *J. Solid State Chem.* **262**, 313 (1973).
- ⁷R. Chandra, S. Bjarman, T. Ericsson, L. Häggström, C. Wilkinson, and R. Wappling, *J. Solid State Chem.* **34**, 389 (1980).
- ⁸P. Jernberg, A. A. Yousif, L. Häggström, and Y. Andersson, *J. Solid State Chem.* **53**, 313 (1984).
- ⁹N. H. Dung, Z. Q. Ou, L. Caron, L. Zhang, D. T. C. Thanh, G. A. de Wijs, R. A. de Groot, K. H. J. Buschow, and E. Brück, *Advanced Energy Materials* **1**, 1215 (2011).
- ¹⁰N. H. Dung, L. Zhang, Z. Q. Ou, L. Zhao, L. van Eijck, A. M. Mulders, M. Avdeev, E. Suard, N. H. van Dijk, and E. Brück, *Phys. Rev. B* **86**, 045134 (2012).
- ¹¹M. D. Kuz'min and M. Richter, *Phys. Rev. B* **76**, 092401 (2007).
- ¹²A. Fujita, Y. Akamatsu, and K. Fukamichi, *J. Appl. Phys.* **85**, 4756 (1999).
- ¹³A. Fujita and H. Yako, *Scr. Mater.* **67**, 578 (2012).
- ¹⁴K. G. Sandeman, *Scr. Mater.* **67**, 566 (2012).
- ¹⁵H. Yamada and K. Terao, *Phase Transitions* **75**, 231 (2002).
- ¹⁶E. K. Delczeg-Czirjak, L. Bergqvist, O. Eriksson, Z. Gercsi, P. Nordblad, L. Szunyogh, B. Johansson, and L. Vitos, *Phys. Rev. B* **86**, 045126 (2012).
- ¹⁷L. Severin, L. Haggstrom, L. Nordstrom, Y. Andersson, and B. Johansson, *J. Phys.: Condens. Matter* **7**, 185 (1995).
- ¹⁸E. K. Delczeg-Czirjak, L. Delczeg, M. P. J. Punkkinen, B. Johansson, O. Eriksson, and L. Vitos, *Phys. Rev. B* **82**, 085103 (2010).
- ¹⁹E. K. Delczeg-Czirjak, Z. Gercsi, L. Bergqvist, O. Eriksson, L. Szunyogh, P. Nordblad, B. Johansson, and L. Vitos, *Phys. Rev. B* **85**, 224435 (2012).
- ²⁰X. Liu, J. P. Liu, Q. Zhang, and Z. Altounian, *Phys. Lett. A* **377**, 731 (2013).
- ²¹A. Barcza, Z. Gercsi, K. S. Knight, and K. G. Sandeman, *Phys. Rev. Lett.* **104**, 247202 (2010).
- ²²Z. Gercsi, K. Hono, and K. G. Sandeman, *Phys. Rev. B* **83**, 174403 (2011).
- ²³Z. Gercsi and K. G. Sandeman, *Phys. Rev. B* **81**, 224426 (2010).
- ²⁴J. B. Staunton and B. L. Gyorffy, *Phys. Rev. Lett.* **69**, 371 (1992).
- ²⁵H. Fujii, S. Komura, T. Takeda, T. Okamoto, Y. Ito, and J. Akimitsu, *J. Phys. Soc. Jpn.* **46**, 1616 (1979).
- ²⁶G. Kresse and J. Furthmuller, *Phys. Rev. B* **54**, 11169 (1996).
- ²⁷J. P. Perdew, K. Burke, and M. Ernzerhof, *Phys. Rev. Lett.* **77**, 3865 (1996).
- ²⁸S. H. Vosko, L. Wilk, and M. Nusair, *Can. J. Phys.* **58**, 1200 (1980).
- ²⁹Z. Gercsi and M. Hudl (private communication).
- ³⁰K. Momma and F. Izumi, *J. Appl. Crystallogr.* **41**, 653 (2008).